Supporting Information

Magnetic Anisotropy along a Series of Lanthanide Polyoxometalates with Pentagonal Bipyramidal Symmetry

Jing Li, [†,‡,§] *Chen Yuan,* [†,§] *Li Yang,* [‡] *Ming Kong,* [‡] *Jing Zhang,* [‡] *Jing-Yuan Ge,* [‡] *Yi-Quan Zhang,*,*[†] *and You Song*,*[‡]

† Jiangsu Key Laboratory for NSLSCS, School of Physical Science and Technology, Nanjing Normal University, Wenyuan Road 1, Nanjing 210023, P. R. China

‡ State Key Laboratory of Coordination Chemistry, Collaborative Innovation Center of Advanced Mirostructures, School of Chemistry and Chemical Engineering, Nanjing University, Xianlin Road 163, Nanjing 210023, P. R. China

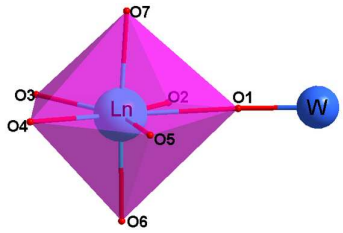

Figure S1. The ligand environment of Ln ions, O1 comes from the polyoxometalate ion, and other coordinated O atoms come from N-Methyl pyrrolidone. The length of Ln-O7 bond is longer than Ln-O6.

Table S1. Crystal data and structure refinement for **Tb**, **Dy**, **Ho**, **Tm**, **Yb**, **Lu**.

	Tb	**Dy**	**Ho**	**Tm**	**Yb**	**Lu**
Empirical formula	$C_{30}H_{54}N_6O_{46}PTbW_{12}$	$C_{30}H_{54}N_6O_{46}PDyW_{12}$	$C_{30}H_{54}N_6O_{46}PHoW_{12}$	$C_{30}H_{54}N_6O_{46}PTmW_{12}$	$C_{30}H_{54}N_6O_{46}PYbW_{12}$	$C_{30}H_{54}N_6O_{46}PLuW_{12}$
*M*r	3630.88	3634.34	3636.89	3640.89	3645.00	3646.93
T(K)	296(2)	296(2)	296(2)	296(2)	296(2)	296(2)
λ(Å)	0.71073	0.71073	0.71073	0.71073	0.71073	0.71073
Crystal system	triclinic	triclinic	triclinic	triclinic	triclinic	triclinic
Space group	$P\bar{1}$	$P\bar{1}$	$P\bar{1}$	$P\bar{1}$	$P\bar{1}$	$P\bar{1}$
a (Å)	12.114	12.124	12.119	12.002	12.062	12.087
b (Å)	13.591	13.611	13.615	13.542	13.592	13.589
c (Å)	22.209	22.227	22.373	22.138	22.241	22.214
α (°)	80.28	80.29	80.25	80.02	80.16	80.20
β (°)	85.34	85.37	85.54	85.67	85.68	85.55
γ (°)	67.55	67.54	67.67	67.55	67.30	67.37
V (Å^3)	3330.7	3340.9	3365(3)	3274.9	3314.3	3319.0
Z	2	2	2	2	2	2
*D*c (g/cm^3)	3.620	3.613	3.589	3.692	3.652	3.649

$F(000)$	3224	3226	3228	3232	3234	3236
$2\theta_{max}(°)$	25.50	25.005	25.499	25.005	25.498	25.003
R_{int}	0.0553	0.0731	0.0873	0.0461	0.0801	0.0857
GOF on F^2	1.096	1.114	0.990	1.119	1.191	1.101
R_1	0.0760	0.0850	0.0825	0.1357	0.1070	0.0848
wR_2	0.2018	0.2257	0.2081	0.3413	0.2596	0.2099
CCDC number	1526936	1526938	1526934	1526939	1526935	1526937

Table S2. Shape measurements of complex (the smallest value is showed in RED) in the SHAPE program. The closer the number is to zero the closer the geometry is to the perfect defined geometry. Code: HP-Heptagon (D_{7h}), HPY- Hexagonal pyramid (C_{6v}), PBPY- Pentagonal bipyramid (D_{5h}), COC- Capped octahedron (C_{3v}), CTPR- Capped trigonal prism (C_{2v}) , JPBPY- Johnson pentagonal bipyramid J13 (D_{5h}), JETPY- Johnson elongated triangular pyramid J7 (C_{3v}).

	HP	HPY	PBPY	COC	CTPR	JPBPY	JETPY
complexes	34.204	25.451	0.278	6.818	5.15	3.101	23.198

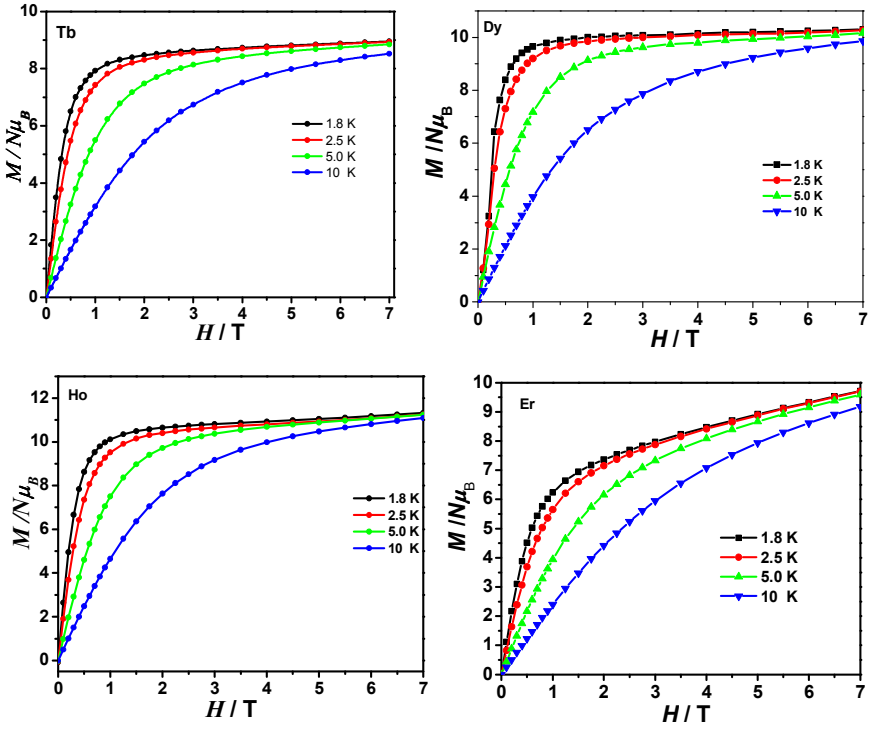

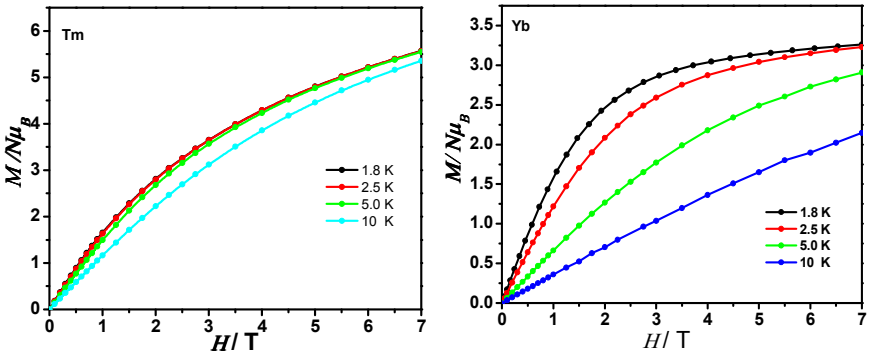

Figure S2. Field dependence of magnetization under low temperature for **Tb**, **Dy**, **Ho**, **Er**, **Tm**, **Yb**.

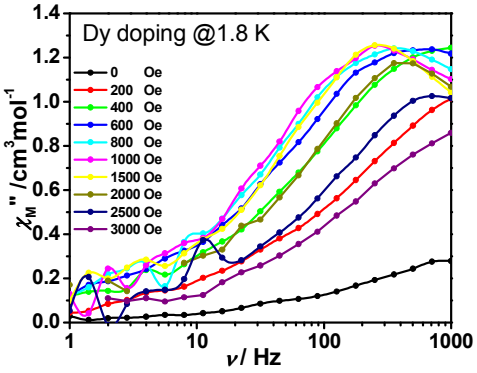

Figure S3. Variable-frequency out-of-phase χ_M'' components of the ac magnetic susceptibility collected for a microcrystalline sample of **Dy-doping** at 1.8 K under different applied dc fields.

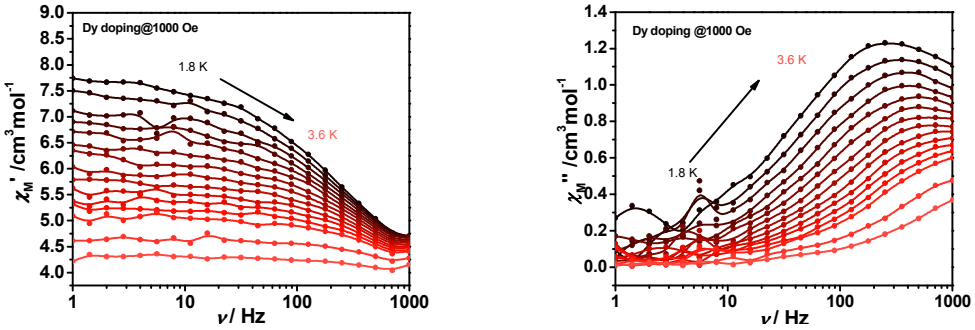

Figure S4. Frequency dependence of the in-phase (χ_M') and out-of-phase (χ_M'') AC susceptibilities under 1000 Oedc field (1–999 Hz, by MPMS Squid VSM) at indicated temperatures for **Dy-doping**.

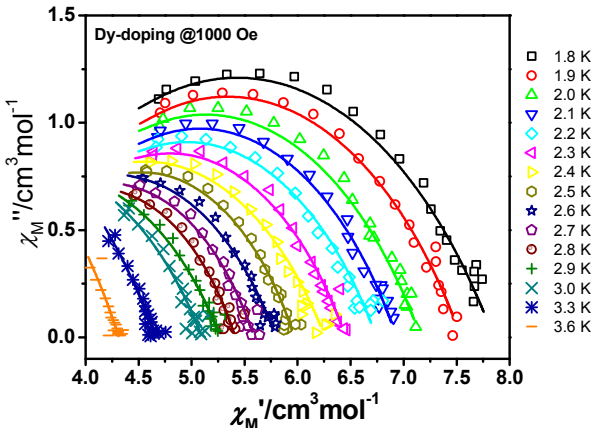

Figure S5. Variable temperature Cole–Cole plots under 1000 Oe dc field at indicated temperatures for complex **Dy-doping**.

Table S3. Analysis of Cole-Cole plot of **Dy-doping** under 1000 Oe dc field.

T/K	χ_s	χ_t	τ	α	R
1.8	3.02E+00	7.85E+00	4.78E-04	4.06E-01	1.57E-01
1.9	3.15E+00	7.54E+00	4.55E-04	3.96E-01	1.12E-01
2	3.11E+00	7.16E+00	3.71E-04	3.94E-01	2.46E-01
2.1	3.22E+00	6.93E+00	3.61E-04	3.83E-01	7.96E-02
2.2	3.16E+00	6.74E+00	3.17E-04	3.99E-01	1.48E-01
2.3	3.14E+00	6.45E+00	2.68E-04	3.89E-01	7.02E-02
2.4	2.91E+00	6.26E+00	1.97E-04	4.20E-01	1.09E-01
2.5	3.12E+00	5.97E+00	2.00E-04	3.68E-01	7.60E-02
2.6	2.81E+00	5.80E+00	1.35E-04	4.02E-01	5.51E-02
2.7	2.90E+00	5.59E+00	1.28E-04	3.76E-01	8.15E-02
2.8	2.87E+00	5.41E+00	1.10E-04	3.66E-01	7.84E-02
2.9	2.23E+00	5.27E+00	5.36E-05	4.19E-01	5.25E-02
3	1.84E+00	5.10E+00	3.38E-05	4.20E-01	7.08E-02
3.3	6.92E-12	4.66E+00	7.99E-06	4.02E-01	5.15E-02
3.6	1.10E-12	4.31E+00	5.59E-06	3.59E-01	3.83E-02

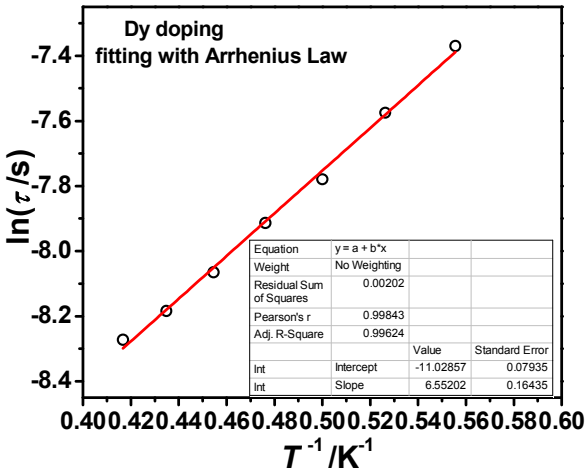

Figure S6. Arrhenius plots of ln(τ) vs. the inverse temperature T^{-1}, as calculated from data at a dc field of 1000 Oe. Red line show the fit of the data to the Arrhenius expression $\tau = \tau_0 \exp(U_{eff}/kT)$ with $U_{eff} = 6.55$ K.

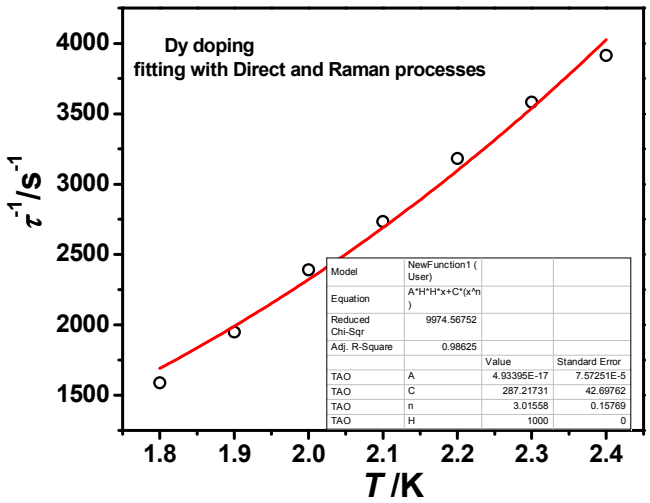

Figure S7. τ^{-1} vs. the temperature T, calculated from data at dc field of 1000 Oe . Red lines show fit to the data using $\tau^{-1} = A H^2 T + CT^n$ with n =3.01, which is smaller than the expected values for Kramer ion SMMs where $n \geq 4$. It is unbefitting.

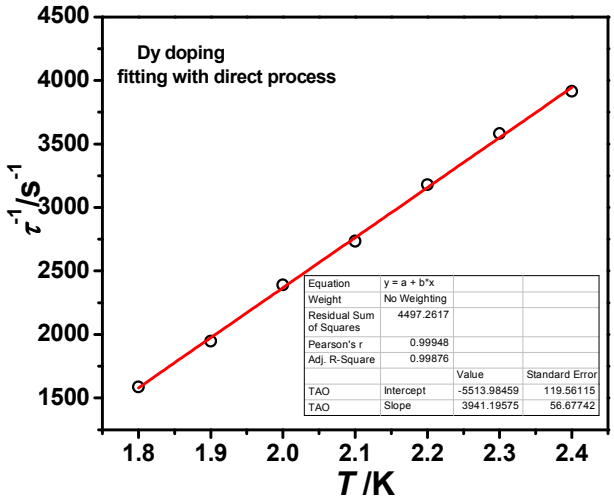

Figure S8. τ^{-1} vs. the temperature T, calculated from data at dc field of 1000 Oe . Red lines show fit to the data using $\tau^{-1} = A H^2 T +$ constant.

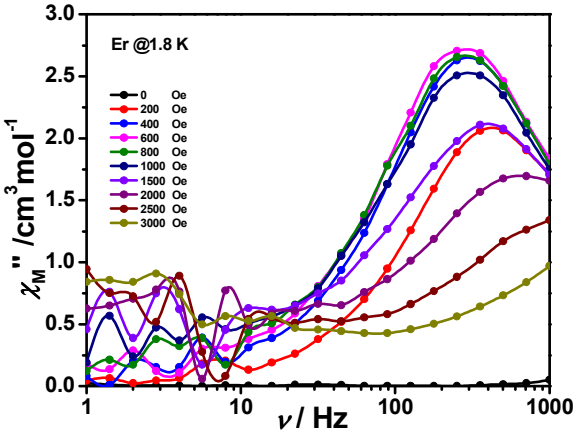

Figure S9. Variable-frequency out-of-phase χ_M'' components of the ac magnetic susceptibility collected for a microcrystalline sample of **Er** at 1.8 K under different applied dc fields.

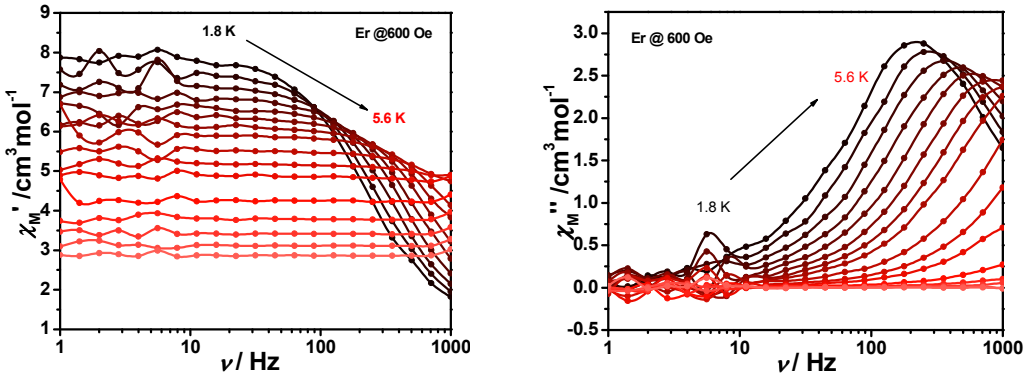

Figure S10. Frequency dependence of the in-phase (χ_M') and out-of-phase (χ_M'') AC susceptibilitiesunder 600 Oe dc field (1–999 Hz, by MPMS Squid VSM) at indicated temperatures for **Er**.

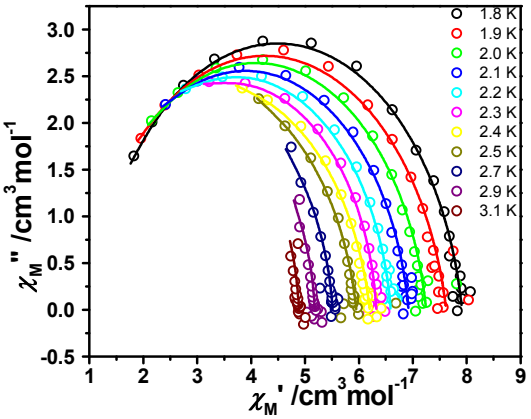

Figure S11. Variable temperature Cole–Cole plots under 600 Oe dc field at indicated temperatures for complex **Er**.

Table S4. Analysis of Cole-Cole plot of **Er** under 600 Oe dc field.

T/K	χ_S	χ_t	τ	α	R

1.8	1.07E+00	7.91E+00	6.91E-04	1.08E-01	1.40E-01
1.9	8.94E-01	7.62E+00	5.39E-04	1.27E-01	5.74E-01
2	9.30E-01	7.25E+00	4.25E-04	1.05E-01	5.11E-01
2.1	8.82E-01	6.92E+00	3.27E-04	9.65E-02	1.82E-01
2.2	8.59E-01	6.59E+00	2.52E-04	7.96E-02	4.61E-01
2.3	9.07E-01	6.32E+00	1.97E-04	6.06E-02	2.06E-01
2.4	3.26E-01	6.20E+00	1.29E-04	1.19E-01	2.26E-01
2.5	2.35E-02	5.95E+00	9.39E-05	1.13E-01	7.39E-01
2.7	5.59E-13	5.51E+00	5.77E-05	7.16E-02	1.81E-01
2.9	3.11E-13	5.18E+00	3.68E-05	5.36E-02	1.24E-01
3.1	2.66E-13	4.89E+00	2.32E-05	4.19E-02	1.35E-01

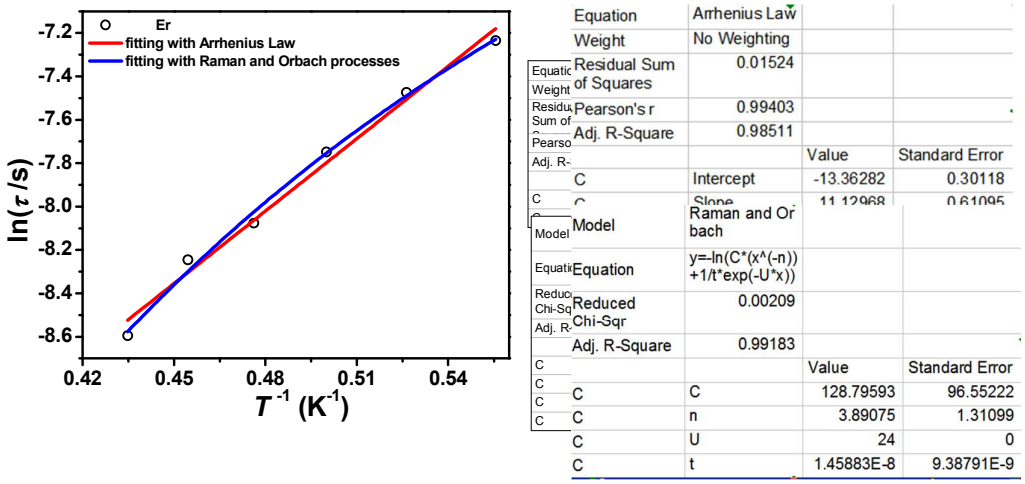

Equation	Arrhenius Law		
Weight	No Weighting		
Residual Sum of Squares	0.01524		
Pearson's r	0.99403		
Adj. R-Square	0.98511		
		Value	Standard Error
C	Intercept	-13.36282	0.30118
C	Slope	11.12968	0.61095

Model	Raman and Orbach		
Equation	y=-ln(C*(x^(-n)) +1/t*exp(-U*x))		
Reduced Chi-Sqr	0.00209		
Adj. R-Square	0.99183		
		Value	Standard Error
C	C	128.79593	96.55222
C	n	3.89075	1.31099
C	U	24	0
C	t	1.45883E-8	9.38791E-9

Figure S12. Plots of ln(τ) vs. the inverse temperature T^{-1}, as calculated from data at a dc field of 600 Oe for **Er**. Red line shows the fit of the data to the Arrhenius expression $\tau = \tau_0 \exp(U_{eff}/kT)$ with U_{eff} = 11.12 K, and blue line shows the fit with $\tau^{-1} = CT^n + \tau_0^{-1}\exp(-U/kT)$ with n = 3.89, U = 24 K.

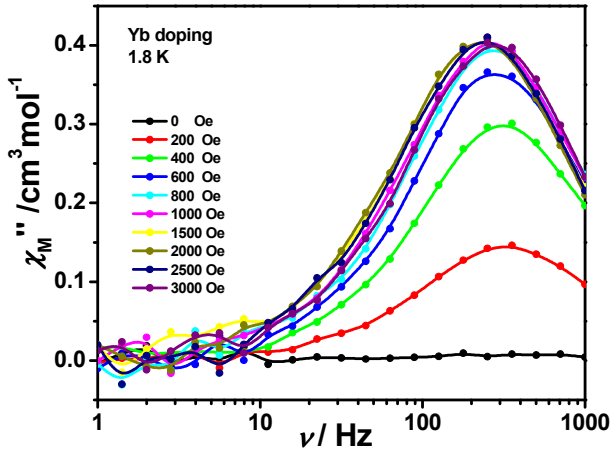

Figure S13. Variable-frequency out-of-phase χ_M'' components of the ac magnetic susceptibility collected for a microcrystalline sample of **Yb-doping** at 1.8 K under different applied dc fields.

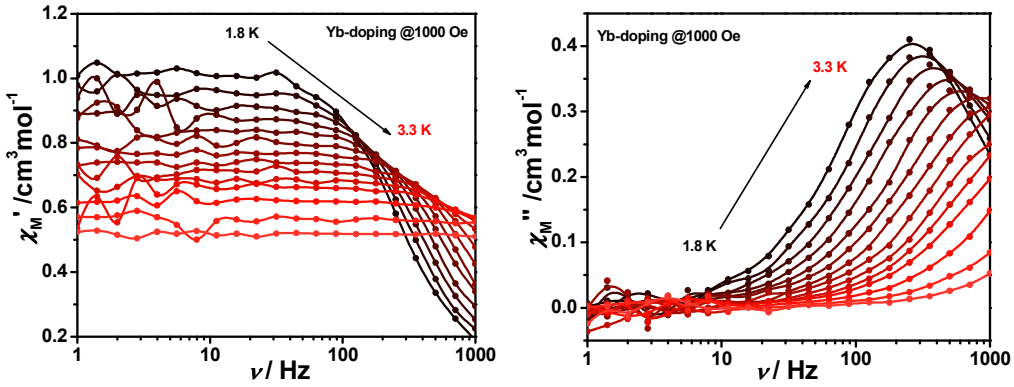

Figure S14. Frequency dependence of the in-phase (χ_M') and out-of-phase (χ_M'') AC susceptibilities under 1000 Oe dc field (1–999 Hz, by MPMS Squid VSM) at indicated temperatures for **Yb-doping**.

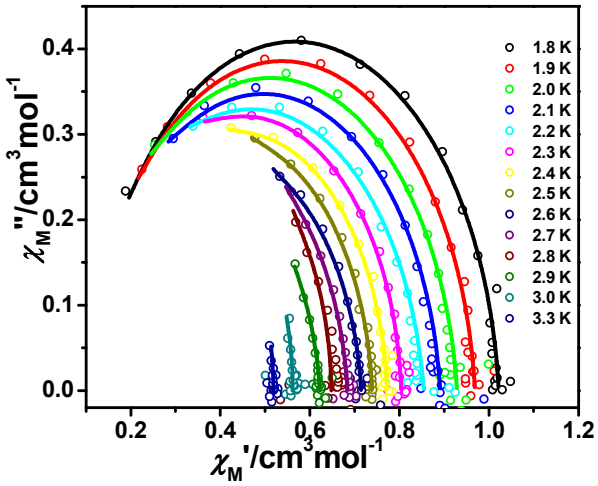

Figure S15. Variable temperature Cole–Cole plots under 1000 Oe dc field at indicated temperatures for complex **Yb-doping**.

Table S5. Analysis of Cole-Cole plot of **Yb-doping** under 1000 Oe dc field.

T /K	χ_S	χ_t	τ	α	R
1.8	1.11E-01	1.02E+00	6.11E-04	5.89E-02	3.04E-03
1.9	1.08E-01	9.68E-01	4.97E-04	5.96E-02	4.15E-03
2	9.35E-02	9.29E-01	3.97E-04	7.41E-02	1.13E-02
2.1	1.02E-01	8.91E-01	3.29E-04	7.15E-02	1.46E-02
2.2	8.42E-02	8.54E-01	2.54E-04	9.00E-02	1.23E-02
2.3	1.03E-01	8.04E-01	2.13E-04	4.56E-02	2.98E-03
2.4	1.14E-01	7.72E-01	1.72E-04	4.56E-02	4.66E-03
2.5	8.58E-02	7.39E-01	1.30E-04	5.13E-02	1.23E-03
2.6	8.19E-02	7.15E-01	9.88E-05	7.13E-02	7.60E-03
2.7	5.57E-11	6.84E-01	6.94E-05	7.12E-02	3.39E-03
2.8	7.44E-11	6.48E-01	5.92E-05	1.77E-02	2.87E-02
2.9	7.20E-14	6.22E-01	3.82E-05	7.53E-02	2.10E-03

3	1.40E-13	5.62E-01	2.51E-05	7.01E-14	6.27E-03
3.3	1.94E-13	5.18E-01	1.61E-05	9.02E-14	1.91E-03

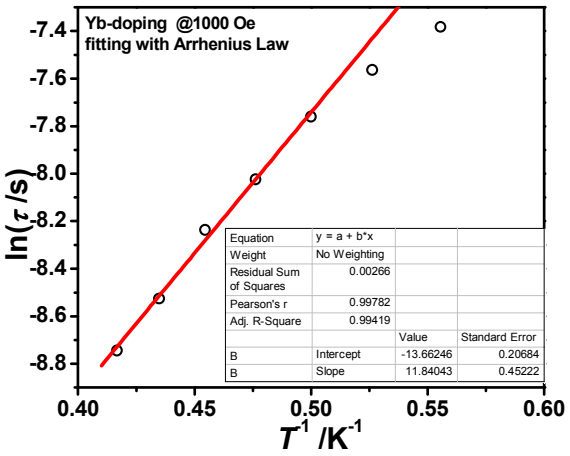

Figure S16. Arrhenius plots of ln(τ) vs. the inverse temperature T^{-1}, as calculated from data at a dc field of 1000 Oe. Red line show the fit of the data to the Arrhenius expression $\tau = \tau_0 \exp(U_{eff}/kT)$ with U_{eff} = 11.84 K.

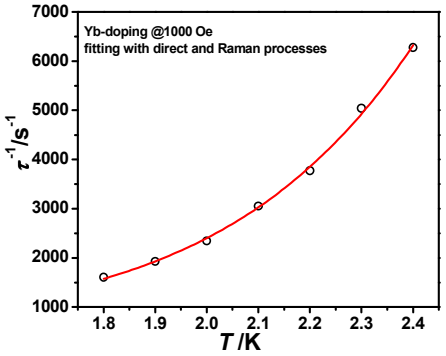

Model	NewFunction (User)		
Equation	y=A*H*H*x+C*(x^n)		
Reduced Chi-Sqr	6493.09734		
Adj. R-Square	0.9978		
		Value	Standard Error
A	A	5.22195E-4	1.10867E-4
A	H	1000	0
A	C	9.02173	5.55002
A	n	7.23156	0.64317

Figure S17. τ^{-1} vs. the temperature T, calculated from data at dc field of 1000 Oe . Red lines show fit to the data using $\tau^{-1} = A H^2 T + C T^n$ with n = 7.23, which is all in accordance with the expected values for Kramer ion SMMs where n ≥ 4.

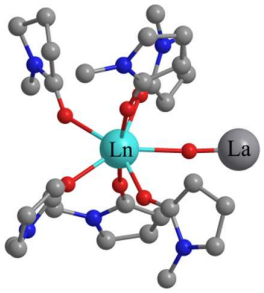

Figure S18. Calculated Ln fragment of complexes **Tb**, **Dy**, **Ho**, **Er**, **Tm**, **Yb**. H atoms are omitted for clarity.

Table S6. The fitted Ln-Ln magnetic interactions (J_{total}) with respect to the pseudospin $\tilde{s}$ = 1/2 of the Ln ions, and the intermolecular magnetic interactions (zJ').

	Tb	Dy	Ho	Er	Tm	Yb
J_{total} / cm^{-1}	0.36	−0.25	−0.16	−0.40	−0.04	−0.01
zJ' / cm^{-1}	−0.01	−0.04	0.03	−0.02	−0.40	−0.70

Table S7. Calculated energies (cm^{-1}), $\boldsymbol{g}$ (g_x, g_y, g_z) tensors and m_J values of the lowest spin-orbit states of individual Ln fragments from complexes **Tb**, **Dy**, **Ho**, **Er**, **Tm**, **Yb**.

	Tb			Dy			Ho		
	E	***g***	m_J	*E*	***g***	m_J	*E*	***g***	m_J
1	0.0 0.8	0.000 0.000 17.376	±6	0	0.042 0.083 19.460	±15/2	0.0 0.2	0.000 0.000 19.475	±8
2	97.7 106.5	0.000 0.000 14.221	±5	182.7	0.451 0.605 16.246	±13/2	92.8 96.2	0.000 0.000 16.071	±7
3	212.0 248.2	0.000 0.000 10.725	±4	331.4	2.607 4.530 12.413	±11/2	114.0 115.1	0.000 0.000 18.110	±1
4	306.3		0	372.1	1.323 1.778 14.815	±5/2	133.3 145.9	0.000 0.000 12.224	±6
5	353.4 369.9	0.000 0.000 12.986	±1	451.9	4.151 4.290 9.001	±9/2	190.2 203.1	0.000 0.000 10.152	±5
6	530.1 531.5	0.000 0.000 17.566	±2	518.5	2.610 3.374 14.377	±7/2	228.8		0
7	722.8 722.9	0.000 0.000 17.760	±3	643.5	0.088 0.689 18.520	±1/2	245.7 252.2	0.000 0.000 13.877	±2
8				682.5	0.173 0.735 19.037	±3/2	294.3 295.9	0.000 0.000 18.283	±3
9							314.9 315.6	0.000 0.000 18.468	±4

	Er			Tm			Yb		
	E	***g***	m_J	*E*	***g***	m_J	*E*	***g***	m_J
1	0.0	0.560 5.129 12.660	±15/2	0.0 6.1	0.000 0.000 12.060	±6	0.0	0.399 0.932 7.098	±7/2
2	16.6	0.385 4.196 11.896	±5/2	24.9 33.9	0.000 0.000 10.859	±5	113.0	0.377 1.779 6.122	±3/2
3	65.9	3.970 5.384 10.169	±1/2	174.7		0	387.9	1.961 3.128 4.420	±5/2
4	109.6	1.668 2.855 9.137	±11/2	216.9 238.8	0.000 0.000 5.355	±2	589.4	0.534 0.597 7.499	±1/2
5	176.3	0.025 1.409 11.829	±13/2	284.8 298.5	0.000 0.000 10.779	±4			
6	247.5	8.332 6.043 1.659	±7/2	405.8 417.5	0.000 0.000 11.303	±3			
7	258.9	10.088 6.243 1.141	±3/2	629.1 630.7	0.000 0.000 13.758	±1			
8	340.8	0.047 0.103 17.387	±9/2						
9									

Table S8. Calculated energies (cm^{-1}), ***g*** (g_x, g_y, g_z) tensors and m_J values of the lowest eight spin-orbit states of individual Dy fragment from complex **Dy** with the different Dy-O1, Dy-O6 and Dy-O7 distances (Å). The Dy-O1, Dy-O6 and Dy-O7 distances of **Dy** derivative are 2.456 Å, 2.222 Å, and 2.223 Å, respectively.

	Dy-I			**Dy-II**			**Dy-III**		
Dy-O1	2.302			2.302			2.302		
Dy-O6	2.222			2.100			2.300		
Dy-O7	2.223			2.100			2.300		
	E	***g***	m_J	*E*	***g***	m_J	*E*	***g***	m_J
1	0.0	0.014 0.024 19.666	±15/2	0.0	0.030 0.052 19.624	±15/2	0.0	0.010 0.016 19.674	±15/2
2	246.3	0.202 0.264 16.654	±13/2	250.6	0.004 0.772 15.956	±13/2	244.7	0.162 0.216 16.627	±13/2

3	446.3	1.563 1.839 13.620	±11/2	293.9	0.363 0.784 17.542	±7/2	455.1	1.325 1.466 13.512	±11/2
4	537.7	0.083 0.916 16.215	±7/2	437.5	1.183 2.624 12.209	±11/2	606.7	3.046 4.334 9.866	±9/2
5	605.2	2.155 3.173 8.457	±9/2	530.6	1.541 3.522 8.846	±9/2	682.7	1.694 1.883 15.287	±5/2
6	678.4	3.277 5.542 12.512	±5/2	609.2	10.773 6.996 3.204	±5/2	736.9	2.246 3.040 14.243	±7/2
7	817.4	0.011 0.704 18.517	±1/2	808.0	0.010 0.855 17.806	±1/2	851.5	0.111 0.695 18.720	±1/2
8	857.5	0.121 0.708 19.016	±3/2	847.7	0.143 0.792 18.654	±3/2	890.3	0.165 0.428 19.202	±3/2

	Dy-IV		
Dy-O1	2.302		
Dy-O6	2.400		
Dy-O7	2.400		
	E	***g***	m_J
1	0.0	0.006 0.010 19.674	±15/2
2	244.7	0.128 0.176 16.575	±13/2
3	462.2	1.214 1.518 13.266	±11/2
4	624.9	4.599 4.997 8.599	±9/2
5	752.6	3.034 3.650 10.600	±3/2

6	852.9	0.546 0.715 17.174	±7/2
7	920.7	0.012 0.360 17.412	±1/2
8	966.8	0.120 0.457 17.847	±5/2

Table S9. Selected bond lengths (Å) and angles (deg) in model complexes **Dy-I** to **Dy-IV** and complex **Dy**.

	Dy	**Dy-I**	**Dy-II**	**Dy-III**	**Dy-IV**
O1-Dy	2.459	2.302	2.302	2.302	2.302
O2-Dy	2.316	2.316	2.316	2.316	2.316
O3-Dy	2.298	2.298	2.298	2.298	2.298
O4-Dy	2.227	2.227	2.227	2.227	2.227
O5-Dy	2.383	2.383	2.383	2.383	2.383
O6- Dy	2.222	2.222	2.222	2.222	2.222
O7-Dy	2.222	2.222	2.222	2.222	2.222
O1- Dy -O2	70.79	70.79	70.79	70.79	70.79
O2- Dy -O3	75.56	75.56	75.56	75.56	75.56
O3- Dy -O4	73.18	73.18	73.18	73.18	73.18
O4- Dy -O5	72.99	72.99	72.99	72.99	72.99
O1- Dy -O5	68.67	68.67	68.67	68.67	68.67
O1- Dy -O6	82.11	82.11	82.11	82.11	82.11
O1- Dy -O7	93.58	93.58	93.58	93.58	93.58

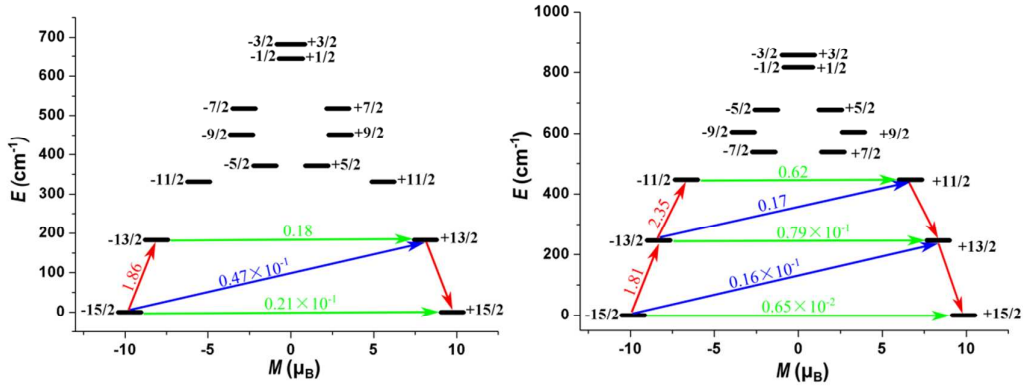

Dy

Dy-I

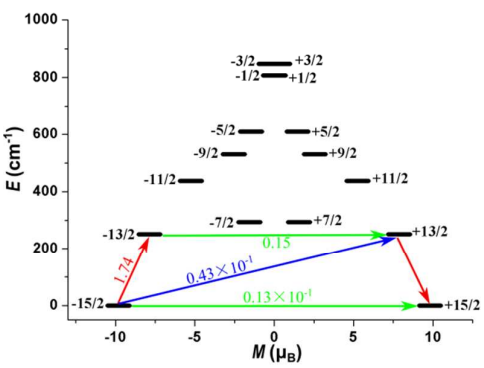

Dy-II

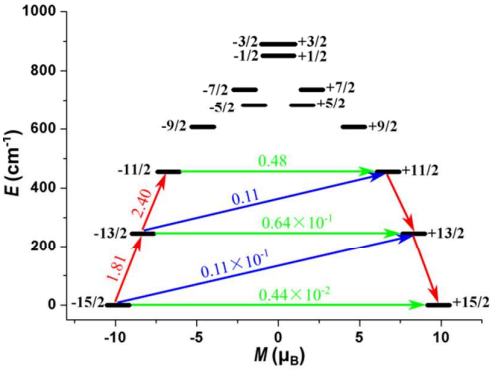

Dy-III

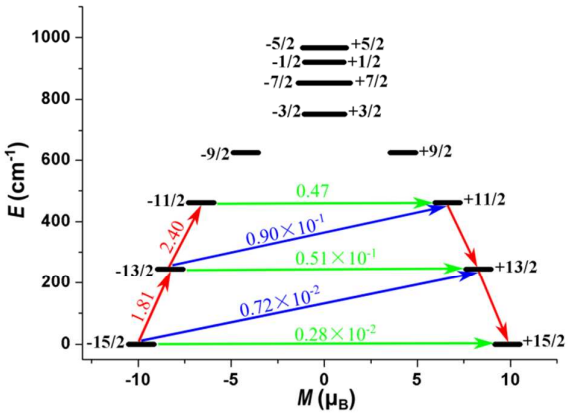

Dy-IV

Figure S19. Magnetization blocking barriers in complexes **Dy** to **Dy-IV**. The thick black lines represent the Kramers doublets as a function of their magnetic moment along the magnetic axis. The green lines correspond to diagonal quantum tunneling of magnetization (QTM); the blue line represent off-diagonal relaxation process. The numbers at each arrow stand for the mean absolute value of the corresponding matrix element of transition magnetic moment.

Figure S20. Calculated Dy^{III} fragment of complexes **Dy-V** to **Dy-IX**; H atoms are omitted.

Table S10. Selected bond lengths (Å) and angles (deg) in model complexes **Dy-V** to **Dy-IX** and reference complex.

	Dy-V	**Dy-VI**	**Dy-VII**	**Dy-VIII**	**Dy-IX**	**Ref. 9b**
O1-Dy	2.10	2.20	2.35	2.4	2.5	2.21
O2-Dy	2.10	2.20	2.35	2.35	2.35	2.35
O3-Dy	2.36	2.36	2.36	2.36	2.36	2.36
O4-Dy	2.34	2.34	2.34	2.34	2.34	2.34
O5-Dy	2.35	2.35	2.35	2.35	2.35	2.35
O6- Dy	2.36	2.36	2.36	2.36	2.36	2.36
O7-Dy	2.33	2.33	2.33	2.33	2.33	2.33
O1- Dy -O2	179.0	179.0	179.0	179.0	179.0	179.0
O2- Dy -O3	87.5	87.5	87.5	87.5	87.5	87.5
O3- Dy -O4	70.7	70.7	70.7	70.7	70.7	70.7
O4- Dy -O5	71.4	71.4	71.4	71.4	71.4	71.4
O1- Dy -O5	89.5	89.5	89.5	89.5	89.5	89.5
O1- Dy -O6	90.4	90.4	90.4	90.4	90.4	90.4
O1- Dy -O7	89.8	89.8	89.8	89.8	89.8	89.8
O6- Dy -O7	72.7	72.7	72.7	72.7	72.7	72.7

Table S11. Calculated energy levels (cm^{-1}), $\boldsymbol{g}$ (g_x, g_y, g_z) tensors and m_J values of the lowest Kramers doublets (KDs) of complexes **Dy-V** to **Dy-IX**.

KDs	**Dy-V (2.1)**			**Dy-VI (2.2)**			**Dy-VII (2.35)**		
	E/cm^{-1}	$\boldsymbol{g}$	m_J	E/cm^{-1}	$\boldsymbol{g}$	m_J	E/cm^{-1}	$\boldsymbol{g}$	m_J
1	0.0	0.000 0.000 19.884	±15/2	0.0	0.000 0.000 19.882	±15/2	0.0	0.000 0.000 19.881	±15/2
2	672.2	0.000 0.000 16.899	±13/2	578.7	0.000 0.000 16.951	±13/2	461.0	0.000 0.000 17.010	±13/2
3	1245.9	0.004 0.005 14.078	±11/2	1046.6	0.006 0.008 14.170	±11/2	800.0	0.021 0.025 14.249	±11/2
4	1642.1	0.562 0.094 11.069	±9/2	1355.1	0.650 1.055 11.695	±9/2	1003.3	1.400 2.600 10.531	±9/2
5	1723.8	0.360 2.304 17.283	±1/2	1438.0	1.292 3.804 15.999	±1/2	1059.1	1.700 5.715 12.558	±3/2
6	1810.1	9.390 8.600 3.780	±7/2	1505.3	3.468 6.536 10.502	±3/2	1117.8	2.445 4.536 11.825	±5/2
7	1888.3	1.146 1.403 15.625	±5/2	1578.4	0.060 0.358 16.190	±7/2	1186.1	0.039 0.127 16.551	±7/2
8	1929.2	0.112 0.812 18.820	±3/2	1632.7	0.271 0.377 19.505	±5/2	1248.6	0.090 0.098 19.741	±1/2

KDs	**Dy-VIII (2.4)**			**Dy-IX (2.5)**		
	E/cm^{-1}	$\boldsymbol{g}$	m_J	E/cm^{-1}	$\boldsymbol{g}$	m_J
1	0.0	0.000 0.000 19.881	±15/2	0.0	0.000 0.000 19.879	±15/2
2	426.8	0.000 0.001 17.025	±13/2	364.6	0.001 0.001 17.046	±13/2
3	729.1	0.033 0.042 14.255	±11/2	600.8	0.101 0.144 14.198	±11/2
4	901.7	1.984 4.110 9.906	±9/2	713.0	3.429 6.389 10.765	±9/2

5	947.3	10.575 6.518 1.262	±7/2	746.9	1.040 2.947 8.770	±3/2
6	1005.0	2.167 4.131 12.181	±3/2	801.3	1.492 2.997 12.949	±5/2
7	1071.4	0.096 0.150 16.652	±5/2	863.3	0.196 0.338 16.846	±7/2
8	1134.2	0.051 0.060 19.770	±1/2	923.9	0.002 0.013 19.811	±1/2

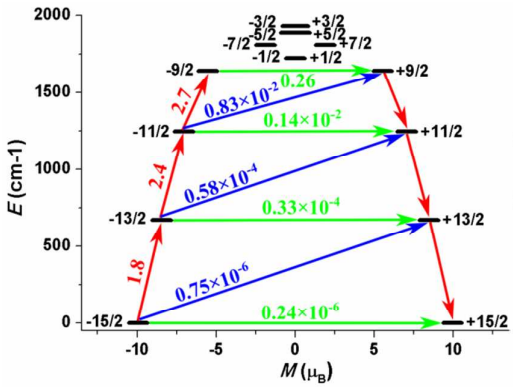

Dy-V

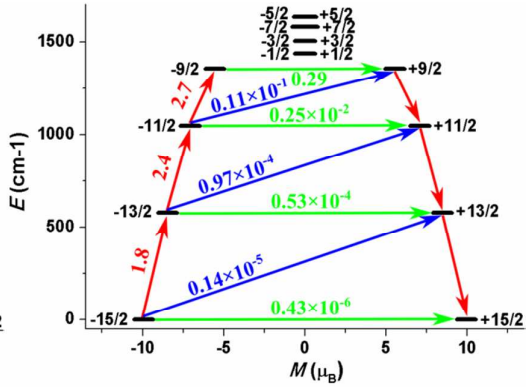

Dy-VI

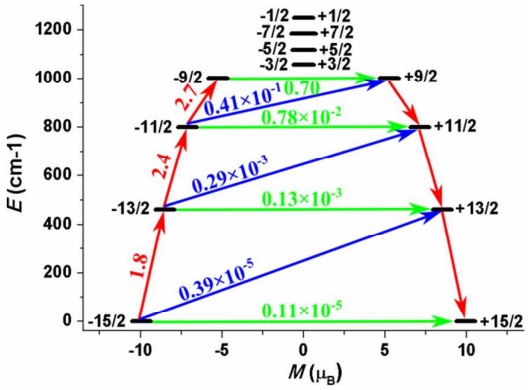

Dy-VII

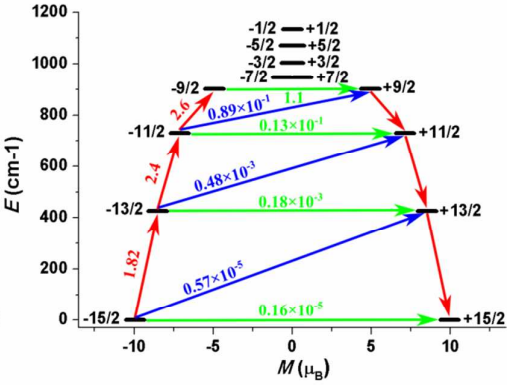

Dy-VIII

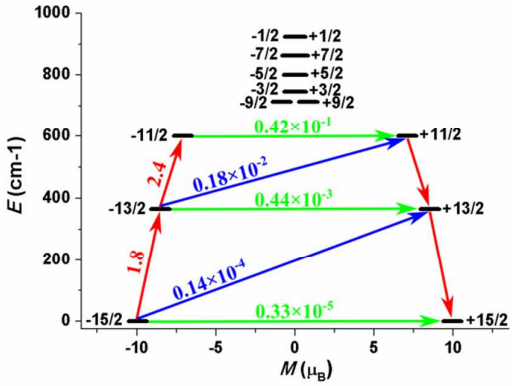

Dy-IX

Figure S21. Magnetization blocking barriers in complexes **Dy-V to Dy-IX**. The thick black lines represent the Kramers doublets as a function of their magnetic moment along the magnetic axis. The green lines correspond to diagonal quantum tunneling of magnetization (QTM); the blue line represent off-diagonal relaxation process. The numbers at each arrow stand for the mean absolute value of the corresponding matrix element of transition magnetic moment.

Reference

S1 Karlstrom, G.; Lindh, R.; Malmqvist, P. A.; Roos, B. O.; Ryde, U.; Veryazov, V.; Widmark, P. O.; Cossi, M.; Schimmelpfennig, B.; Neograd y, P.; Seijo, L. MOLCAS: a Program Package for Computational Chemistry, *Comput. Mater. Sci*. **2003**, *28*, 222–239.

S2 Seijo, L.; Barandiarán, Z.; Computational Chemistry: Reviews of Current Trends; World Scientific, Inc.: Singapore, **1999**; 455−152.